



Review

The influence of dust on extreme precipitation at a large city in North China[☆]

Taichen Feng^{a,b}, Tiangang Yuan^c, Jiahui Cao^d, Zhikuan Wang^e, Rong Zhi^f, Zhiyuan Hu^{a,b,*}, Jianping Huang^{g,h}

^a School of Atmospheric Sciences, Key Laboratory of Tropical Atmosphere-Ocean System, Ministry of Education, Sun Yat-sen University, Zhuhai 519082, China

^b Southern Marine Science and Engineering Guangdong Laboratory, Zhuhai 519082, China

^c Earth and Environmental Sciences Programme and Graduation Division of Earth and Atmospheric Sciences, Faculty of Science, The Chinese University of Hong Kong, Shatin, Hong Kong SAR, China

^d College of Atmospheric Sciences, Lanzhou University, Lanzhou, China

^e College of Physical Science and Technology, Yangzhou University, Yangzhou, China

^f National Climate Center, China Meteorological Administration, Beijing, China

^g Collaborative Innovation Center for Western Ecological Safety, Lanzhou University, Lanzhou 730000, China

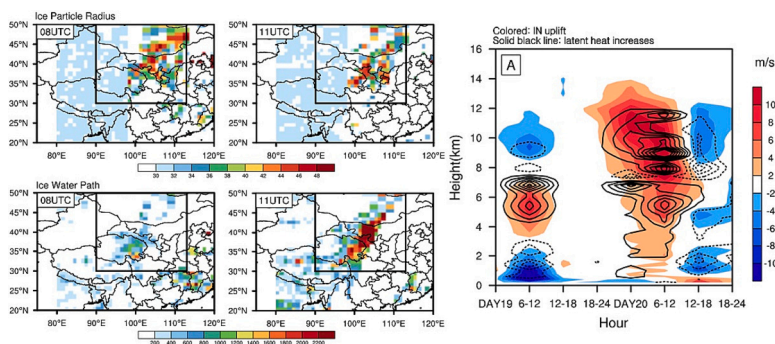
^h Key Laboratory for Semi-Arid Climate Change of the Ministry of Education, College of Atmospheric Sciences, Lanzhou University, Lanzhou 730000, China



HIGHLIGHTS

- Long-range transported dust triggered extreme precipitation over downstream regions.
- Dust glaciated the supercooled cloud as ice nuclei at an altitude of 7.5 km.
- Dust significantly increased ice nuclei uplift rate before the precipitation.

GRAPHICAL ABSTRACT



ARTICLE INFO

Editor: Jianmin Chen

Keywords:

Dust aerosol

Extreme precipitation

ABSTRACT

In recent decades, the Beijing-Tianjin-Hebei city cluster is experiencing rapid urbanization along with economic booming. Meanwhile, these cities are suffering the influence of extreme precipitation and dust storms. In this study, the impact of dust aerosol on extreme precipitation that occurred in Beijing during 19–21 July 2016 is investigated using both satellite retrievals and Weather Research and Forecasting model coupled to Chemistry (WRF-Chem) model simulations. Results reveal that the dust particles can increase extreme precipitation by

[☆] This work was supported by the National Natural Science Foundation of China (grant number 42130610, 41975088 and 42075105), the Guangdong Basic and Applied Basic Research Foundation (grant no. 2022A1515010585), and the 2022 “Future Earth” Early Career Fellowship from Future Earth Global Secretariat Hub China.

* Corresponding author at: School of Atmospheric Sciences, Key Laboratory of Tropical Atmosphere-Ocean System, Ministry of Education, Sun Yat-sen University, Zhuhai 519082, China.

E-mail address: huzhiyuan@mail.sysu.edu.cn (Z. Hu).

<https://doi.org/10.1016/j.scitotenv.2023.165890>

Received 28 March 2023; Received in revised form 25 July 2023; Accepted 27 July 2023

Available online 2 August 2023

0048-9697/© 2023 The Authors. Published by Elsevier B.V. This is an open access article under the CC BY license (<http://creativecommons.org/licenses/by/4.0/>).

promoting the formation of ice clouds and enhancing convections. The dust is lifted into the upper troposphere (>10 km) via strong convection and affects the physical process of precipitation after long-range transport. It further transforms the supercooled water into the middle and high levels of ice nuclei (IN). These promote the formation of ice clouds according to the decreased effective radius of IN and increased ice water path, respectively. Along with sufficient water vapor transport and strong convergence, the formation of IN could release more latent heat and further strengthen convection development. Thus, the precipitation amount in southern Beijing is almost enhanced by 40 % (>80 mm). This study will provide a deep insight into understanding the causes of urban extreme precipitation.

1. Introduction

Precipitation extremes frequently occur in many regions of the world with global warming (Wang et al., 2021; Nashwan and Shahid, 2022; Ma et al., 2022a, 2023a). Generally, precipitation extremes are usually caused by a short-term heavy rainfall or a large cumulative rainfall in the long duration (Wu and Luo, 2019). For example, the amount of precipitation reached >70 mm in 1 h, 100 mm in 6 h, or 150 mm in 24 h is defined as extreme precipitation in Beijing areas (https://www.beijing.gov.cn/zhengce/zwmc/202202/t20220221_2613323.html). In recent decades, many cities in China have been affected by extreme precipitation events (Trenberth et al., 2003; Liu et al., 2009; Shiu et al., 2012; Ma et al., 2019, 2022b, 2023b) with the decrease of light precipitation (Su et al., 2020). More than that, the extreme hourly precipitation and maximum hourly precipitation in summer over North China present an increasing trend (Xiao et al., 2016), which indicates that the extreme precipitation events occurring in North China will increase.

At present, the causes and influencing mechanisms of extreme precipitation are not very clearly and remain to be further studied (Emori and Brown, 2005; Li et al., 2016; Li et al., 2019). Aerosols and urbanization are recognized as two major factors causing extreme precipitation. Firstly, urbanization caused by human activities significantly changes surface characteristics and makes cities not only heat sources but also aerosol sources. The accelerated urbanization obviously influences the local weather, including precipitation (Shem and Shepherd, 2009; Sun and Zhao, 2021; Sun et al., 2023). Moreover, the related urban heat island effect can alter regional evaporation (Wienert and Kuttler, 2005), wind field (Hjelmfelt, 1982; Shen et al., 2019, 2021) and atmospheric circulation (Shepherd and Burian, 2003; Baik et al., 2007; Lei et al., 2008). In addition, urban geomorphology also affects the formation of thunderstorms (Haberlie et al., 2015), and changes the amount and location of precipitation (Shepherd et al., 2002; Niyogi et al., 2011), which results in increasing intensity of extreme precipitation (Miao et al., 2011).

Secondly, with the development of urbanization, emitted aerosols affect precipitation through radiation (Charlson et al., 1992; Hansen et al., 1997) and cloud microphysics (Khain et al., 2009; Tao et al., 2012). The sixth Assessment Report of the Intergovernmental Panel on Climate Change has stated that aerosols have significant impacts on precipitation mainly via two aspects: aerosol-cloud interaction (ACI) and aerosol-radiation interaction (ARI) (IPCC, 2021). Rosenfeld (1999) reported that aerosols affected the vertical development of mixed-phase in warm clouds and inhibit precipitation (Li et al., 2011), while the effect of aerosol on precipitation is complex in deep convective clouds. When aerosols inhibit precipitation, smaller cloud droplets are lifted by updrafts and form ice particles, which leads to more latent heat releasing and enhances convection related with cloud condensation nucleus (CCN) concentration (Lin et al., 2006; Fan et al., 2007; Rosenfeld et al., 2008). In particular, black carbon emitted from urbanization can increase precipitation at night through “aerosol-enhanced condition instability” (Fan, 2018). Besides, the effect of aerosol radiation on precipitation in three different megacities in eastern China is also evident, which is worthy of attention too (Sun and Zhao, 2021). Thus, aerosols play a key role in the intensity and uncertainty of extreme precipitation (Fan et al., 2015; Lee et al., 2016). The increased spatial variability of

aerosol concentration with urbanization will likely increase the frequency and intensity of extreme precipitation events (Lee et al., 2018).

Mineral dust is one of the main components of aerosols in the atmosphere (IPCC, 2021; Hu et al., 2019a, 2020, 2023), which is recognized as the most important source of ice-nucleating particles due to their high ice-nucleating efficiency (Engelstaedter et al., 2006; Heymsfield, 2007; Husar et al., 2001; Uno et al., 2009; Zhang et al., 2019; Che et al., 2021; Zhao et al., 2022). Previous studies proved that mineral dust aerosol contributed to ice nuclei (IN) concentrations and improved precipitation efficiency (Fan et al., 2014; Muhlbauer and Lohmann, 2009) in many regions, even though these areas were far away from the dust sources (DeMott et al., 2003; Richardson et al., 2007). The cloud model also suggested that dust affected IN could accelerate the ice-forming process and promote the development of precipitation when the dust presents above the -5°C level (Yin and Chen, 2007). The dust aerosol reduced the radius of ice particles in deep convective clouds but increased the cloud ice water path (IWP) and cloud optical depth, which could further promote the development of clouds and leads to extreme precipitation in India (Yuan et al., 2021). More research emphasized that the dust aerosol over the Tibetan Plateau could affect the development of convective clouds and the expansion of the IWP, and further lead to the precipitation over downstream regions (Liu et al., 2019; Zhao et al., 2020). However, the effects of dust aerosol on urban extreme precipitation still need to be examined.

During 19–21 July 2016, an extreme precipitation event occurred in North China. Before the extreme precipitation occurred, a dust plume was observed, which may affect the convective cloud mixing process. Moreover, sufficient water vapor provided beneficial conditions for this event (Sun, 2017; Tian et al., 2017), which could significantly increase the precipitation under the influence of dust aerosol (Creamean et al., 2013). In this event, Beijing suffered severe damage on 20 July 2016 (Beijing “7.20” extreme precipitation), which became another record-breaking extreme precipitation event after the “7.21” rainstorm in 2012. What's worse, the precipitation amount reaching exceeded the “7.21” event and the influenced areas were more wide. In addition, Beijing-Tianjin-Hebei was experiencing urbanization with rapid economic development. To what extent, therefore, did the dust aerosol contribute to the extreme precipitation event in 2016 under the background of urbanization? Addressing the question is essential for enhancing our understanding of the formation and development of extreme precipitation in urbanized regions of North China. This study employed the WRF-Chem model to examine the effects of aerosols and urbanization on extreme precipitation. Combined with reanalysis and satellite data, the influencing mechanism of dust aerosols on precipitation was emphatically studied. The model has been widely used to investigate the mechanisms through which different aerosols influence precipitation (Zhao et al., 2012; Naeger, 2018). The study also used Emission Reduction Impacts (ERI) methods to compare simulation differences between scenarios with full and reduced emission sources (Thunis et al., 2019). Similar approaches have been applied successfully in previous study to aerosols effects on precipitation (Zhong et al., 2015).

2. Data and methodology

2.1.1. WRF-Chem model

The WRF-Chem model (v3.5.1) updated by the University of Science and Technology of China (USTC) (Hu et al., 2022) is used in this. A single-layer Urban Canopy Model (UCM) has been coupled, which is conducted to represent the momentum and energy exchange between the atmosphere and urban surface (Chen, 2011). The Model for Simulation Aerosol Interactions and Chemistry (MOSAIC) aerosol scheme (Zaveri et al., 2008) has been coupled with the Carbon Bond Mechanism (CBM-Z) photochemical mechanism (Zaveri and Peters, 1999), which is applied to simulate the aerosol radiative properties and complex photolysis rates (Fast et al., 2006). Both the aerosol interaction with radiation (Zhao et al., 2011, 2013a) and aerosol impacts on cloud microphysics (Gustafson Jr. et al., 2007) are considered. Besides, the meteorological and chemistry/aerosol fields are simultaneously simulated in the WRF-Chem model (Fast et al., 2006; Qian et al., 2010; Zhao et al., 2013b; Hu et al., 2016, 2019b). The Rapid Radiative Transfer Model (RRTMG) longwave and shortwave radiation solutions (Mlawer et al., 1997; Iacono et al., 2000) are used to represent aerosol radiative feedbacks (Zhao et al., 2011), and the Kain-Fritsch (new Eta) cumulus scheme is applied for cumulus parameterization. The YSU (Yonsei University) boundary layer scheme (Hong et al., 2006) and Noah land surface process scheme (Chen and Dudhia, 2001) are used. The Morrison double-moment microphysical schemes described by Morrison et al. (2009) are also applied. In this case, the two one-way nested domains configured in the model are D01 and D02 (Fig. s1). D01 covers most areas in China, the north Indian Ocean, and the western Pacific; D02 covers Beijing and surrounding provinces. The model simulations are performed at 24 km × 24 km, and 4 km × 4 km horizontal resolution with 400 × 260 and 385 × 379 grid cells, respectively. The simulation time was from 0000 UTC (Coordinated Universal Time) 16 July to 0000 UTC 23 July 2016. The data for the initial field and the boundary field are from the global atmospheric reanalysis data, European Centre for Medium-Range Weather Forecasts (ECMWF) interim reanalysis (ERA-Interim).

In this study, the anthropogenic emissions used in the WRF-Chem model supplied from Asian emission inventory (Zhang et al., 2009). The biomass burning emissions with a monthly temporal resolution (van der Werf et al., 2010) were provided by the Global Fire Emissions Database Version 3 (GFEDv3) and vertically distributed following the injection heights were selected from Aerosol Comparison between Observations and Models (AeroCom) project (Dentener et al., 2006). The Goddard Chemical Aerosol Radiation Transport (GOCART) dust emission scheme (Ginoux et al., 2001) provided vertical dust emission fluxes and the emitted dust particles were distributed into the MOSAIC aerosol size bins (Kok, 2011).

2.1.2. Model experiment setting

This study uses WRF-Chem with two nested domains (Fig. s1). The default urban surface is replaced by remote sensing retrieval and the aerosol influence is considered in the control experiment (STD). In the noA test, the default urban surface is replaced by remote sensing retrieval without considering the aerosol effect. In the noAU test, neither the remote sensing retrieval nor the aerosol effects are considered

Table 1
Model test design.

Name	Land-use category	Aerosol effect
STD	New	Yes
noA	New	No
noAU	Default	No

(Table 1). Extreme precipitation in Beijing and its surrounding areas (39.45°N–41.1°N, 115.4°E–117.4°E) is selected for evaluation in different experiments. The simulation results in the innermost area on 19–20 July are analyzed in detail.

2.2. HYSPLIT model description

The Hybrid Single Particle Lagrangian Integrated Trajectory (HYSPLIT) model, developed by the National Oceanic and Atmospheric Administration (NOAA) Air Resources Laboratory, is designed for rapid response in diagnostic case studies or climatological analyses. The model uses the Lagrangian approach for trajectory calculations, employing a moving frame to calculate advection and diffusion as air parcels move from their initial positions (Stein et al., 2015). Recently, thousands of researchers have gained access to run HYSPLIT trajectory simulations for their research projects through the Real-Time Environmental Applications and Display System (READY) (Fan et al., 2020, 2021a,b), a web-based system maintained by ARL (ready.arl.noaa.gov/) (Rolph and Draxler, 1993). In this study, we use products generated from READY to trace the transport pathways of dust aerosols based on archived three-dimensional meteorological data produced by the National Centers for Environmental Prediction Global Data Assimilation System. Multiple locations within the Taklimakan Desert are selected as the initial region to reduce uncertainty in determining atmospheric transport pathways compared to using a single location (Fleming et al., 2012). The forward trajectory simulation is selected, which the simulation time was from 0000 UTC 16 July to 2400 UTC 18 July 2016. It is worth noting that the air parcel heights are relative to the topography since the profiles of meteorological data are linearly interpolated to a topography-following coordinate system (Draxler and Hess, 1998).

2.3. Observation data

The hourly gridded precipitation dataset (version 1.0) was obtained by fusing the China automatic station and Climate Prediction Center (CPC) morphing (CMORPH) precipitation products which are provided by the China Meteorological Data Network and used to evaluate the model simulations (Zhao et al., 2020; Yang et al., 2021a,b,c). The datasets combine the observed hourly precipitation from 30,000 to 40,000 automatic weather stations nationwide after quality control and the global precipitation inversion product of the CMORPH satellite with a resolution of 8 km every 30 min developed by the U.S. Climate Prediction Center. The temporal resolution is 1 h and the spatial resolution is 0.1° × 0.1°.

2.4. Reanalysis data

The Modern-Era Retrospective analysis for Research and Applications, Version 2 (MERRA-2) is developed by Global Modeling and Assimilation Office, which is the latest NASA atmospheric reanalysis dataset (Gelaro et al., 2017). MERRA-2 products show high reliability and wide application prospects for aerosol concentration and distribution (Sun et al., 2019; Ma et al., 2021). At the same time, MERRA-2 data are widely used in aerosol related studies (Zhao et al., 2018a,b; Feng et al., 2020; Yang et al., 2021a,b) and are often selected to evaluate the results of WRF-Chem model (Ukhov et al., 2020; Pistone et al., 2021). In this research, the hourly dust aerosol optical depth (AOD), daily potential height at 500 hPa, and daily wind field at 850 hPa derived from MERRA-2 with a resolution of 0.5° × 0.625° were used to explore the spatial-temporal evolution of dust aerosol transport process, and evaluate model simulations.

2.5. Satellite observations

The Clouds and the Earth's Radiant Energy System (CERES) instruments provide global observations for cloud and radiative flux by

matching the cloud properties from Moderate Resolution Imaging Spectroradiometer (MODIS) onboard Aqua and Terra and geostationary (GEO) satellites (Wielicki et al., 1996). The Synoptic top-of-atmosphere (TOA) and surface fluxes and clouds (SYN) products contain hourly gridded liquid and ice cloud properties such as IWP, ice particle radius (IPR), and cloud phase with a resolution of $1^\circ \times 1^\circ$.

MODIS is a key instrument aboard Terra and Aqua satellites which are viewing the entire Earth's surface every 1 to 2 days, acquiring data in 36 spectral bands or groups of wavelengths. The Absorbing AOD (AAOD) at 500 nm embedded in MODIS true color image has been chosen to represent the distribution of dust aerosol, which is derived from ozone monitoring instrument (OMI) near-ultraviolet (UV) aerosol algorithm (OMAERUV) product retrieved by OMI onboard Aura satellite (Torres, 2008). Moreover, the MODIS Land Cover Type Yearly Global 500 m (MODIS MCD12Q1) products (Friedl et al., 2002), Cropland Extent 1 km Crop Dominance and Global Food-Support Analysis Data (GFSAD1000; Thenkabail et al., 2012) are also used in this study.

2.6. Cloud phase identification

The CALIPSO satellite carried the Cloud-Aerosol Lidar with Orthogonal Polarization (CALIOP) instrument was launched in April 2006. This Lidar primarily retrieves the vertical profile of aerosols and clouds by providing attenuated backscatter at 532 nm and 1064 nm (Cesana et al., 2016). In this study, the orbits crossing central China at 0612 UTC on 17 July 2016 was selected. The CALIPSO level 2 vertical feature mask (VFM) data provides the vertical distribution of water, ice, and oriented ice crystal cloud along the CALIPSO orbit. Previous research found the relationship between cloud mid-layer temperature and Supercooled Water Cloud (SWC) fraction developed an algorithm for SWC by utilizing CALIPSO cloud products (Hu et al., 2010). Based on the relationship between the cloud mid-layer temperature and Supercooled Water Cloud (SWC) fraction, an algorithm for SWC was developed using CALIPSO cloud products (Hu et al., 2010). The algorithm parameterized with Eq. (1) and relevant parameters are listed in Table 2.

$$P(T_{mid}) = C_0 + \sum_i K_i T_{mid}^i \quad (i = 0, 1, 2, 3, 4) \quad (1)$$

$$f(T) = \frac{1}{1 + e^{-p(T)}} \quad (2)$$

where $p(T)$ is a polynomial fitting function between cloud mid-layer temperature and CALIPSO SWC fraction $f(T)$. Therefore, the SWC fraction can be estimated by Eq. (2). Here, we followed Wang et al. (2019) who used the CALIPSO cloud layer mid-temperature to replace the original mid-layer cloud temperature in Hu et al. (2009) and viewed the cloud with SWC fraction $>80\%$ as SWCs.

3. Results

3.1. The simulation and evaluation of extreme precipitation

The “7.20” rainstorm in North China lasted more than three days, and the spatial distribution and intensity of precipitation varied throughout the entire precipitation process. Observational data indicates that (Fig. 1a), on 19 July, there was only sporadic convective precipitation in North China. Subsequently, systematic precipitation <50 mm occurred in the southern part of China and gradually moved from east to north. Subsequently, extreme precipitation occurred in

Table 2

Formula parameter.

C_0	K_i unit: $1/^\circ\text{C}$				
5.3608	$i = 0$	$i = 1$	$i = 2$	$i = 3$	$i = 4$
	0.4025	0.08387	0.007182	2.39×10^{-4}	2.87×10^{-6}

most parts of North China, with the rain belt stretching from southwest to northeast. From 19 to 20 July, precipitation was mainly occurred at the junction of Yanshan and Taihang Mountains, with the maximum precipitation exceeding 125 mm and concentrated near the Taihang Mountains in a strip distribution. Precipitation gradually affected the south-central region of Beijing on 20 July, with the amount exceeding 150 mm and the rain belt turning to a north-south direction. Meanwhile, the precipitation area decreased and the intensity of precipitation increased. After that, the rain belt gradually moved eastward. Fig. 1b indicates that the STD simulation effectively captures the spatial distribution of observed precipitation and accurately reproduces its intensity. Especially in Beijing, the entire precipitation process is basically reproduced.

The spatial evolution characteristics of this precipitation can be divided into three stages. In the first stage, the rain belt turned in a north-south direction and the main precipitation area was Taihang Mountains and its surrounding areas from 2000 UTC 18 to 0200 UTC 20 July. The second stage was from 0200 UTC to 2000 UTC 20 July, as the precipitation moved from east to north. And the main precipitation area gradually leaved the North China while the weather system continued to move from the east to the north. The third stage was from 2000 UTC 20 to 0800 UTC 21 July, when the main precipitation process in North China was basically ended. This study focuses on the “7.20” extreme precipitation in Beijing and simulates the precipitation process in Beijing from 19 to 20 July.

3.1.1. Model evaluation: wind and circulation field

Before the occurrence of this extreme precipitation, the subtropical high pressure extends west and north, and its ridge line confrontation with the deep low vortex formed by the low trough extending southward to the Taihang Mountains in the eastern part of North China. The circulation system shows an “east-high, west-low” pattern which favors precipitation in North China. The 500 hPa potential height field indicated (Fig. s2a) that a closed vortex with a central value below 5800gpm appearing at the junction of Hebei and Shanxi on 20 July. In addition, previous studies shown that there was a closed low pressure occurring over both 700 hPa and 850 hPa, indicating that this was a deep vortex system from low to high levels, which was also one of the characteristics of the “7.20” extreme precipitation in Beijing. The extreme nature of this precipitation is attributed to the existence of a large-scale system and its slow movement. As the low-pressure system formed and moved northward, the isobars on its east and north sides intensified, especially near Hebei and Beijing, resulting in obvious easterly and southeasterly winds (Zhao et al., 2018a,b).

The STD simulation results exhibited that the upper-air trough (Fig. s2b) was relatively similar to the real situation (Fig. s2a) which was located in the western part of North China on 19 July. The amount of precipitation in a given location is determined by both the precipitation rate and the duration time (Lin, 2007). In the case of this precipitation event, the weather system moved slowly and persisted for an extended period, resulting in a substantial total precipitation accumulation, even though the precipitation rate was relatively low (Fig. 1). However, the simulated trough tilted northeast-southwest more obviously and slightly westward located, which indicated the rain belt from the simulations on 19 July shifted to the west of the real pattern and the trough was deeper with better dynamic conditions. Hence, the intensity of the simulated low vortex shear was stronger than the observation and the precipitation was more concentrated near the shear line (Fig. 1b).

The simulation results of the West Pacific subtropical high indicate that the upper trough continued to move westward and gradually developed into a low vortex, which was located more eastward and northward than in observation. At the lower level, the low vortex was guided by the upper trough and moved northeastward while developing (Fig. s2). The simulated position and intensity of the upper trough differed from the observation, resulting in a more eastward and stronger low vortex in the simulation. Thus, precipitation occurred near the low

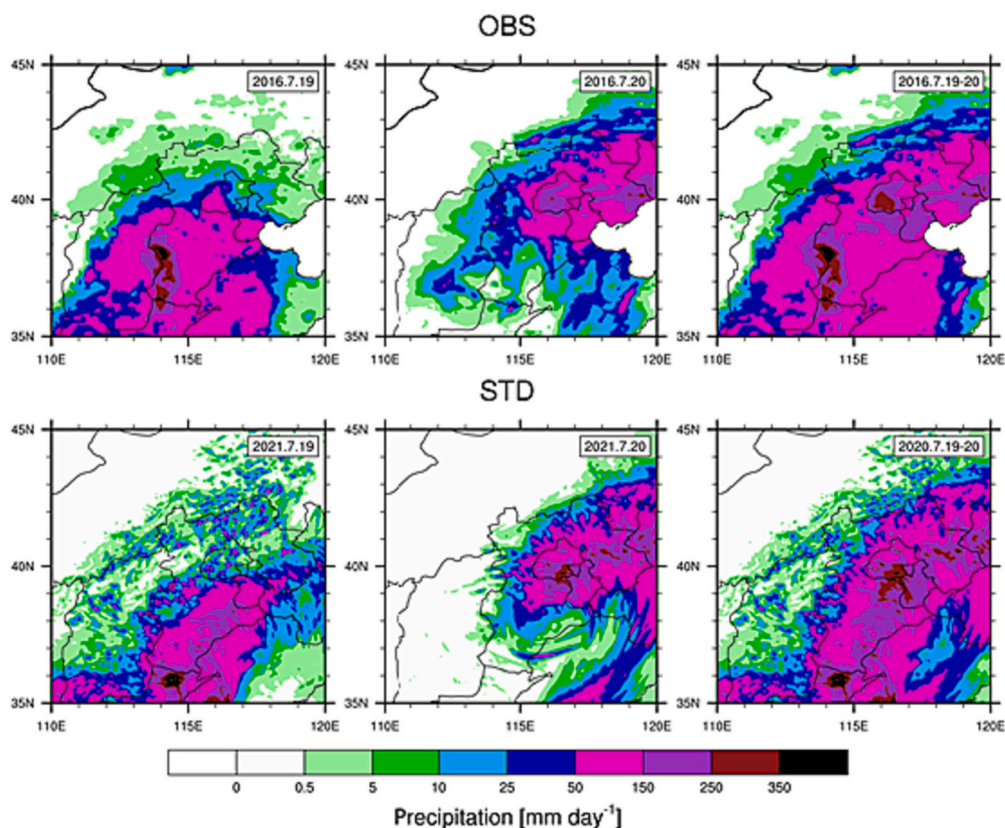


Fig. 1. Daily precipitation and 48-hour accumulated precipitation in D02 region of Beijing from 19 to 20 July 2016 (a) observation results (b) Simulation results of STD test. The coloring represents accumulated precipitation (mm).

vortex shear. However, due to the difference in location, morphology, and intensity of the low vortex, Beijing was near the shear line (warm shear) and influenced by easterly winds in observation (Fig. s3a), while it was controlled by northeasterly winds in the STD simulation. The simulated lower-level low vortex was closer to Beijing, causing its impact on precipitation in addition to the shear line (Fig. s3b). This discrepancy may explain the slightly higher simulated precipitation in Beijing compared to the observation (Fig. 1).

3.1.2. Dust aerosol transport processes

This dust is mainly emitted from the Taklamakan Desert and the northwest Gobi desert. Before the start of this precipitation process, there was a significant dust event process in the Taklamakan Desert in China. The MODIS RGB synthetic cloud map shows that the frontal cloud

system reached central Inner Mongolia as well as Gansu province and formed zonal distribution, while a thicker cloud layer was present on 17 July 2016 (Fig. 2). Both the aerosol type and absorptive aerosol optical depth (AAOD) indicated that the dust aerosol was mainly distributed in the Taklamakan Desert, and partly in central Inner Mongolia and north-central Gansu province (Fig. 2a, filled in brown). Due to the influence of satellite temporal resolution and the existence of clouds, satellites cannot observe the dust within the frontal clouds. The MERRA-2 reanalysis further indicates that the dust from the Taklamakan Desert was transported eastward across Gansu and Shaanxi on 14–17 July, and reached North China on 16–17 July when the dust mass decreased to 0.05–0.1 g m⁻² (Fig. s4).

We further used the HYSPLIT model to track the transport of dust aerosol (Fig. 3). Fig. 3b shows that dust from the Taklamakan Desert is

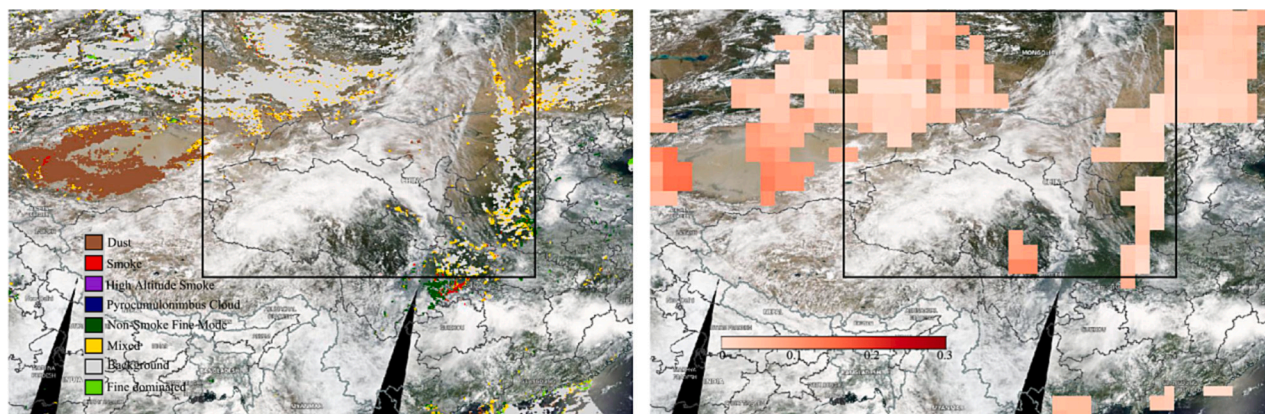


Fig. 2. The corresponding aerosol types obtained by VIIRS deep blue algorithm and AAOD obtained by OMI satellite inversion from the MODIS synthetic cloud image on 17 July 2016. The area in the black box is the dust aerosol assessment area on 17 July.

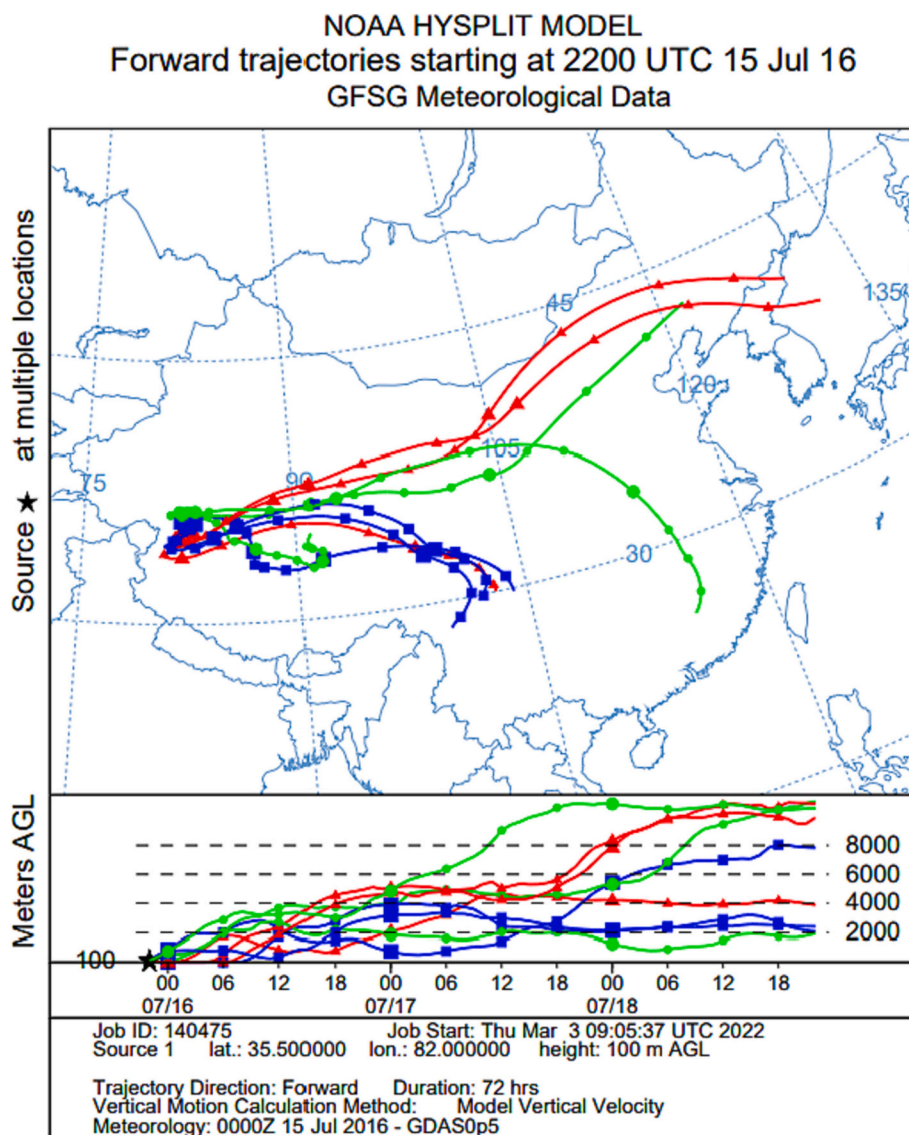


Fig. 3. The forward trajectory simulation of HYSPLIT model with starting positions located in the Taklimakan Desert from 2200 UTC 15 to 2200 UTC 18 July 2016.

mainly transported eastward and divided into three main paths. The first path goes through the Tibetan Plateau and its northern edge to southeastern China and the eastern part of the Tibetan Plateau and Sichuan Basin. The second path goes eastward through Inner Mongolia in Gansu and turns to the southeast of China in central Inner Mongolia. This study mainly analyzes the impact of dust transport on clouds and precipitation in North China (Fig. 3b red line). Within the first few hours, the transport height did not exceed 2 km and was basically concentrated within the boundary layer. Due to the strong sensible heat of the desert, the dust aerosol gradually was lifted to 4–5 km and continuously delivered to the east. At 1800 UTC 17 July, the dust aerosol was lifted rapidly again, reaching 8 km at 0000 UTC 18 July, and over 10 km 6 h later (Fig. 3). Previous analysis of the weather situation of this precipitation had shown that there was an obvious divergence area at 100 hPa height over North China on 20 July, and the strong divergence was conducive to the strengthening of the ascending motion. Therefore, the transport and uplift of dust may be related to the strong upward flow.

3.2. Impact of aerosols and urbanization on extreme precipitation

As shown in Table s1, the effects of aerosols (A), urbanization (U), and urbanization and aerosols (AU) can be quantified by analyzing the

differences among noA-noAU, STD-noA, and STD-noAU, respectively.

There are significant differences between aerosols and urbanization on the spatial distribution of extreme precipitation (Fig. 4). Aerosols contributed to the increase of >80 mm (20–40 %) in precipitation in southern Beijing. But in northern regions of Beijing, although urbanization has a promoting effect on precipitation (Fig. 4c1, c2), the inhibition of aerosols on precipitation is more obvious, with a decrease of >80 mm in most areas, accounting for >40 % of the total precipitation reduction (Fig. 4b1, b2). Urbanization had a suppressive effect on precipitation in southern Beijing, reducing precipitation by 50–80 mm in some areas, and decreasing total precipitation by 10 %–40 % (Fig. 4c1, c2).

The combined influence of aerosols and urbanization (AU) had a notable impact on precipitation in southern Beijing. While urbanization reduced the range of increased precipitation compared to the effect of aerosols alone, it still led to an increase of over 80 mm in some areas in the south and a total precipitation increase of over 40 % (Fig. 4a1, a2). The model results, shown in Fig. 4a1, were consistent with observations, indicating that the main precipitation was concentrated in southern Beijing. Overall, the inhibitory effect of urbanization on precipitation weakened the promoting effect of aerosols, resulting in an increase in precipitation mainly concentrated in southern Beijing. This led to a

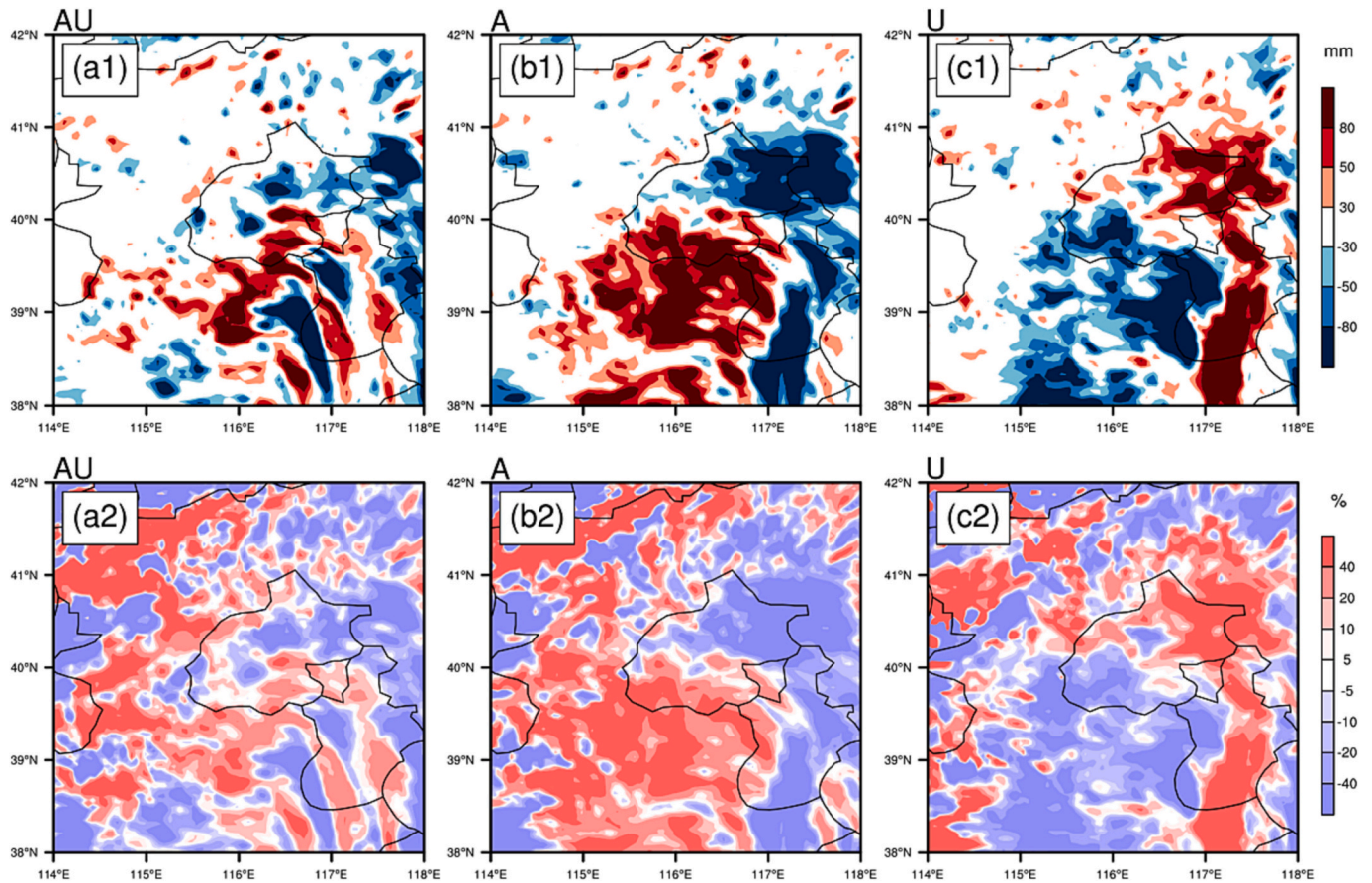


Fig. 4. (a1) Combined effect of aerosol and urbanization on precipitation (AU) (b1) aerosol effect on precipitation (A) (c1) urbanization effect on precipitation (U) (mm). (a2, b2, c2) Same as a1, b1 and c1 but for precipitation contribution percentage (%).

limited precipitation process under the combined effect of aerosols and urbanization.

3.3. Effects of dust on extreme precipitation

3.3.1. Observational analysis of the effects of dust aerosol on IN and IWP

According to Yuan et al. (2021), strong convective processes can lift water vapor to heights above the 0 °C isentropic surface under suitable dynamical conditions and strong water vapor transport. Dust aerosol may play an important role in the development of these clouds. However, due to the lack of IN and condensation nuclei, most of the water vapor forms super-cooled water clouds. When the convective system lifts the dust aerosol to the upper level, some of them are activated into IN,

rapidly transforming SWCs into ice clouds. This results in a decrease in ice cloud radius and an increase in albedo, releasing latent heat and further enhancing the convective system. More water vapor and dust entering the convective clouds can eventually promote convective cloud development.

CALIPSO satellite data showed that dust presented at an altitude of 7.5–12.5 km in Inner Mongolia at 0612 UTC 17 July, especially at an altitude of 7.5 km, 40°N, where dust, SWCs, and ice clouds were present simultaneously (Fig. 5b). From Fig. 2a, the dust aerosol has been transported to Inner Mongolia and Gansu area on the 17 July, which was consistent with the geographic location of dust transport on the 17 July as simulated by the forward trajectory shown in Fig. 3b. Since dust can be the main source of nucleating particles for IN, in addition, the long-

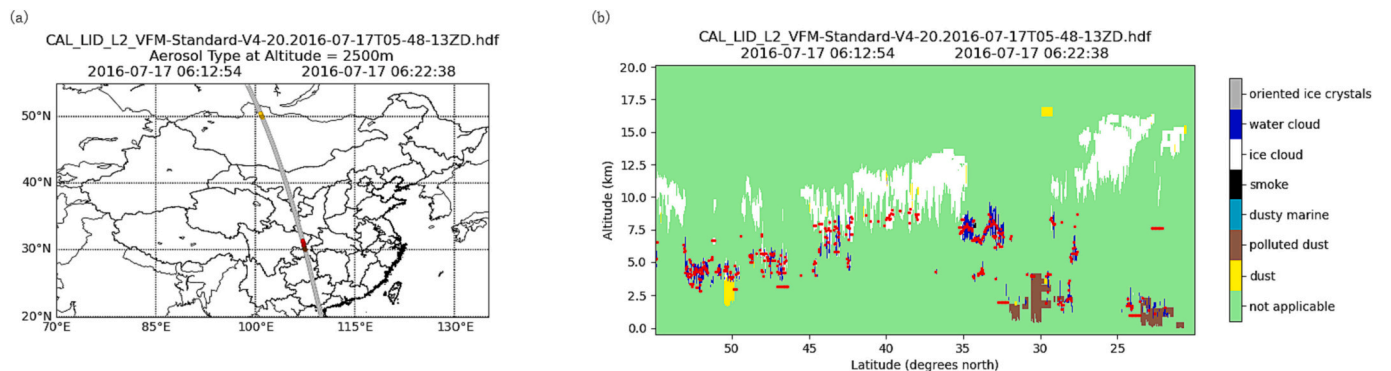


Fig. 5. (a) The gray line is the CALIPSO tracks, (b) the CALIPSO aerosol and cloud types selected from CALIPSO cloud products (red dots are supercooled water clouds).

range dust transport impacted IN (DeMott et al., 2003; Richardson et al., 2007). Therefore, the CERES satellite information in the black box assessment area shows that dust aerosol has a significant impact on IPR and IWP over central Inner Mongolia (Fig. 6). From 0800 UTC to 1100 UTC 17 July, over central Inner Mongolia, the IPR within the whole cloud was affected by dust transport and varied more significantly in the region north of 40°N, which was consistent with the transport path region simulated by the HYSPLIT model on the 17 July. In the 40°N–45°N, 105°E–110°E region, the IPR gradually decreased from 0800 UTC (42–46 μm) to 1100 UTC (below 30 μm). In contrast, the increase in IWP was extremely significant (Fig. 6b). At 0800 UTC, the IWP was only 200–1000 g m^{-2} over the central Inner Mongolia, but after 3 h, the IWP increased to >2200 g m^{-2} and gradually approached North China with the weather system. The aforesaid suggested that dust particles may act as IN to condense supercooled water and lead to increased ice clouds.

3.3.2. Model simulation analysis of dust aerosol

Observation data are difficult to accurately demonstrate the evolution of dust and clouds. The STD simulation showed that the dust was continuously transported to northern of China during the whole precipitation process. Fig. s5 demonstrates the spatial and temporal evaluation of dust mass loading. During 19 to 20 July, the dust mass in clouds decreased at first and then increased (Fig. s5). At 0000 UTC–1800 UTC 19 July, the dust mass gradually decreased within the clouds around Beijing, at 1800 UTC 19 July, only small amount of dust aerosol existed within clouds over northeastern Hebei (about 0.005–0.02 mg m^{-2}). On 20 July, with the influence of the weather system, the precipitation gradually increased and the dust within the clouds over Beijing and surrounding areas increased rapidly. From 1800 UTC to 0600 UTC 20 July, the dust within the clouds in northern Hebei increased significantly, and the mass had exceeded 0.1 mg m^{-2} . In the following 6 h (0600 UTC–1200 UTC 20 July) the dust located in northern Hebei sharply decreased and almost disappeared (dust mass below 0.0001 mg m^{-2}). However, during 1200 UTC–2400 UTC 20 July, the dust mass in Beijing and Hebei gradually increased again (0.001–0.02 mg m^{-2}). These indicate that dust continued to transport to the Beijing area during precipitation.

Combined with the effect of aerosols on the rate of ice nuclei uplift and latent heat release in Fig. 7a. It can be found that the rate of ice nuclei uplift increased and latent heat was released at 6 km during 0000 UTC–12:00UTC 19 July. On 0000 UTC–0600 UTC 20 July, the ice nuclei uplift rate increased and latent heat was released in the whole atmosphere, especially at 8–12 km, which was consistent with variations of dust mass in Beijing and its surroundings in the model. The height with

the fastest increase in ice nuclei uplift rate (10–12 km) was also consistent with the HYSPLIT results (reaching 10 km altitude in North China).

Therefore, dust aerosol played a key role in the formation of the IN in extreme precipitation. During ice-formation, the released latent heat enhanced convection, the convergent, the uplift of water vapor and dust, which resulted the increased precipitation. However, the effect of dust aerosol on the rate of ice nuclei uplift was not always constant during precipitation. Before the precipitation, dust aerosol results in the increase in IN, the release of latent heat, the enhancement of convection and convergence, which eventually increased precipitation. After that, dust aerosol continued to be transported to the northern China, and no longer acted as effective IN in weak convective systems. Instead, they participated in the precipitation process as cloud condensation nodules. During this precipitation, excessive dust aerosol (1200 UTC–2400 UTC 20 July) reduced the cloud droplet size and suppressed precipitation (Fig. 7a).

In model results, from 0600 UTC to 1200 UTC 20 July, the effect of urbanization on precipitation on the altitude of 4–10 km, played a suppressive role on the rate of IN uplift and latent heat release, which could be assumed that urbanization inhibited the production of IN. In addition, urbanization increased the rate of uplift of low-altitude IN and the release of the latent heat (Fig. 7b). Regarding to the combined influence of urbanization and aerosols, the latent heat released and the increased uplift rate of IN were concentrated in two periods, which were similar to the effect of aerosols on precipitation (Fig. 7a). In contrast, urbanization enhanced the inhibition of the ice nucleation process and reduced the release of latent heat at the end of the precipitation.

4. Discussion and conclusions

In general, Emission Reduction Impacts (ERI) methods, Mass-Transfer methods, and Incremental methods are commonly used for source-apportionment in studies (Thunis et al., 2019; Kranenburg et al., 2013; Kiesewetter et al., 2015). The selection of an appropriate source allocation method is crucial in this study to gain a better understanding of the influence of various aerosols on extreme precipitation. It is important to note that the effects of different aerosol types in the models often exhibit nonlinearity, implying that the impact of an individual aerosol cannot be simply extrapolated linearly to represent the overall aerosol effect. This nonlinearity is similar to that seen in air quality planning research (Thunis et al., 2019). To remove the nonlinearity associated with aerosol effects, the noA test set was employed in this study to eliminate all aerosol influences on the extreme precipitation

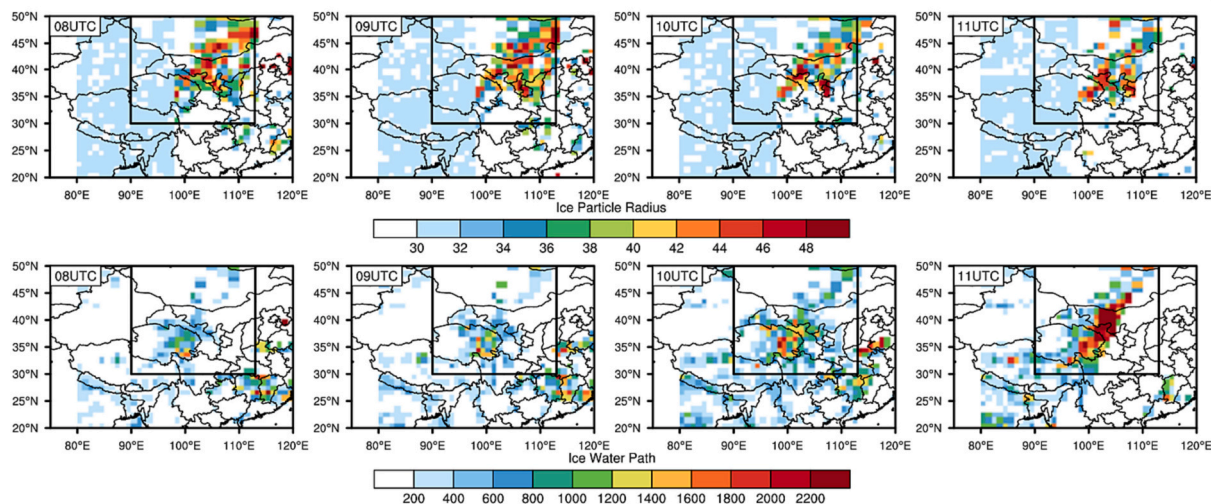


Fig. 6. CERES data from 0800 UTC to 1100 UTC 17 July 2016 (a) IPR (μm) and (b) IWP (g m^{-2}).

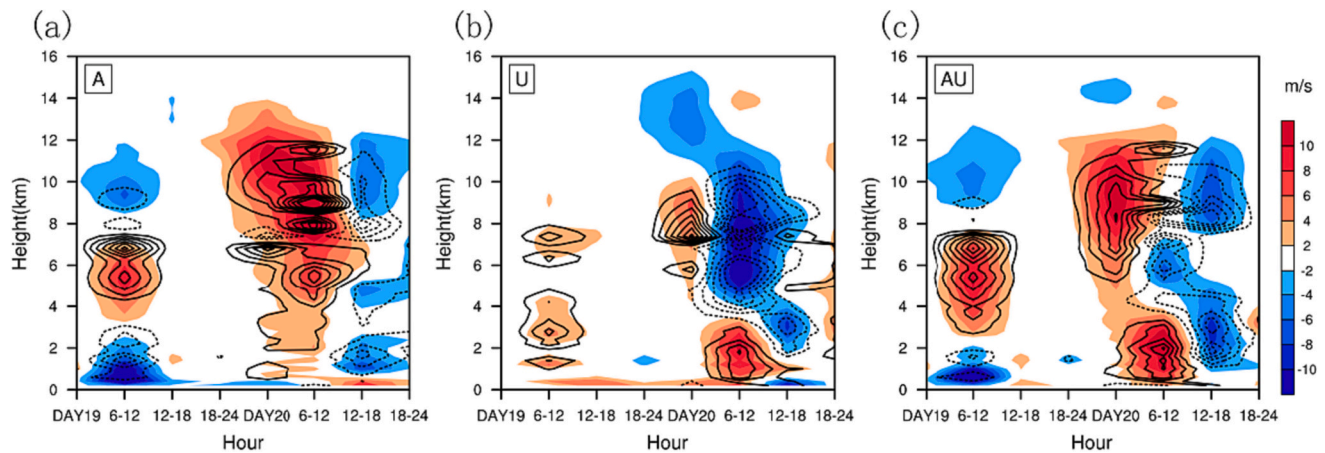


Fig. 7. (a, b, c) The time-height cross section of aerosol (A), urbanization (U), and the combined impact of aerosol and urbanization (AU), respectively. Colored is the rate of IN uplift, (m s^{-1}). The solid black line is the area where latent heat increases; The black dotted line is the area where the latent heat is reduced, (K day^{-1}).

event. However, due to limitations in the selection of the model simulation area, a separate discussion on the influence mechanism of dust aerosols was not conducted. In addition, further detailed investigation is required to distinguish the influence mechanisms of different types of dust aerosols on precipitation (Fan et al., 2014). Future studies will use Mass-Transfer methods to conduct a more comprehensive and detailed analysis.

It is important to consider the uncertainty of the data as it can affect our conclusions. Although CALIOP has been validated with ground-based Lidar in China and has shown reasonable agreements with ground measurements, uncertainties still exist in the vertical profile of aerosol (Wu et al., 2011). The interference of sunlight leads to less reliability of CALIPSO daytime products compared to the nighttime counterparts (Li et al., 2009). The selection of cloud screening and aerosol size distribution models contributes to the large regional differences between MODIS aerosol and cloud products (Jeong, 2005; Li et al., 2009). In addition, significant discrepancies in cloud phase, liquid water path, cloud top height and other parameters in CERES will introduce uncertainties into our results (Minnis et al., 2011a,b). Although AOD assimilation can reduce the bias between MERRA-2 and the observed results, it has limited effectiveness in constraining the aerosol species, absorptivity and vertical structure, and does not significantly improve systematic biases (Buchard et al., 2017). Therefore, to comprehensively evaluate the role of dust aerosol in extreme precipitation within an urbanized context, we use WRF-Chem model to further discuss the influence mechanism of dust aerosol during precipitation process. This approach allows for a more comprehensive understanding of the impact of dust aerosols on extreme precipitation.

The results show that the effects of local aerosols and urban surface changes on precipitation are mainly concentrated within the lower atmosphere. Long-range transport results in lower concentrations of dust aerosol in the atmosphere and higher uplift heights. Therefore, long-range transported dust from the Taklamakan Desert plays a crucial role in the formation of IN and the development of ice clouds during this extreme precipitation. The effect of dust as IN on SWCs and ice clouds is also examined.

Prior to precipitation, dust aerosols that were transported over long distances were gradually lifted to altitudes of >7 km due to surface sensible heat and suitable dynamic conditions. This causes supercooled water clouds to rapidly condense into IN, promoting the formation of ice clouds and resulting in the reduction of IPR and the increase of IWP, which in turn promotes the development of cloud systems. During precipitation, strong convective uplift makes more water vapor and dust aerosol lifted to the condensate layer (above 10 km), which favors the formation of dust IN. The latent heat released from this process further enhance the development of the convection system. However,

urbanization inhibited the production of IN. Braham and Spyers-Duran (1974) pointed out the existence of the deactivation of IN over cities, which may be related to higher temperatures and solarization. Moreover, Chen et al. (2018) showed that none of the urban anthropogenic pollution aerosols contributed to IN concentrations. Therefore, the formation of IN and latent heat release can be considered as the influenced by dust aerosol in this extreme precipitation. At the end of precipitation, the large amount of dust aerosol increases cloud condensation nuclei and reduces cloud droplet particle size, thus inhibiting precipitation. In summary, dust aerosol can enhance extreme precipitation in the context of urbanization, posing a greater threat to urban property and public safety.

CRediT authorship contribution statement

Taichen Feng: Conceptualization, Methodology, Formal analysis, Software, Validation, Writing-original draft, Investigation.

Tiangang Yuan: Methodology, Data analysis.

Jiahui Cao: Software, Data curation.

Zhikuan Wang: Software, Data curation.

Rong Zhi: Methodology, Data analysis.

Zhiyuan Hu: Methodology, Data analysis.

Jianping Huang: Methodology, Supervision, Project administration

Declaration of competing interest

The authors declare that they have no known competing financial interests or personal relationships that could have appeared to influence the work reported in this paper.

Data availability

Data will be made available on request.

Appendix A. Supplementary data

Supplementary data to this article can be found online at <https://doi.org/10.1016/j.scitotenv.2023.165890>.

References

- Baik, J.J., Kim, Y.H., Kim, J.J., Han, J.Y., 2007. Effects of boundary-layer stability on urban heat island-induced circulation. *Theor. Appl. Climatol.* 89 (1), 73–81. <https://doi.org/10.1007/s00704-006-0254-4>.
- Braham, R.R., Spyers-Duran, P., 1974. Ice nucleus measurements in an urban atmosphere. *J. Appl. Meteorol.* 13, 940–945. [https://doi.org/10.1175/1520-0450\(1974\)013<0940:INMIAU>2.0.CO;2](https://doi.org/10.1175/1520-0450(1974)013<0940:INMIAU>2.0.CO;2).

- Buchard, V., Randles, C.A., da Silva, A.M., Darmenov, A., Colarco, P.R., Govindaraju, R., Ferrare, R., Hair, J., Beyersdorf, A.J., Ziemba, L.D., Yu, H., 2017. The MERRA-2 aerosol reanalysis, 1980 onward. Part I: evaluation and case studies. *J. Clim.* 30, 6851–6872. <https://doi.org/10.1175/JCLI-D-16-0613.1>.
- Cesana, G., Chepfer, H., Winker, D., Getzewich, B., Cai, X., Jourdan, O., 2016. Using insitu airborne measurements to evaluate three cloud phase products derived from CALIPSO. *J. Geophys. Res.-Atmos.* 121 (10), 5788–5808. <https://doi.org/10.1002/2015jd024334>.
- Charlson, R.J., Schwartz, S.E., Hales, J.M., 1992. Climate forcing by anthropogenic aerosols. *Science* 255 (5043), 423.
- Che, Y., Zhang, J., Zhao, C., Fang, W., Xue, W., Yang, W., Ji, D., Dang, J., Duan, J., Sun, J., Shen, X., Zhou, X., 2021. A study on the characteristics of ice nucleating particles concentration and aerosols and their relationship in spring in Beijing. *Atmos. Res.* 247, 105196. <https://doi.org/10.1016/j.atmosres.2020.105196>.
- Chen, F., 2011. The integrated WRF/urban modelling system: development, evaluation, and applications to urban environmental problems. *Int. J. Climatol.* 31 (2), 273–288. <https://doi.org/10.1002/joc.2158>.
- Chen, F., Dudhia, J., 2001. Coupling an advanced land surface–hydrology model with the Penn State–NCAR MM5 modeling system. Part I: model implementation and sensitivity. *Mon. Weather Rev.* 129 (4), 569–585. [https://doi.org/10.1175/1520-0493\(2001\)129<0569:Caalsh>2.0.Co;2](https://doi.org/10.1175/1520-0493(2001)129<0569:Caalsh>2.0.Co;2).
- Chen, J., Wu, Z.J., Augustin, B.S., 2018. Ice-nucleating particle concentrations unaffected by urban air pollution in Beijing, China. *Atmospheric Chemistry and Physics* 18 (5), 3523–3539.
- Creamean, J.M., Suski, K.J., Rosenfeld, D., Cazorla, A., DeMott, P.J., Sullivan, R.C., 2013. Dust and biological aerosols from the Sahara and Asia influence precipitation in the western US. *Science* 339 (6127), 1572–1578. <https://doi.org/10.1126/science.1227279>.
- DeMott, P.J., Sassen, K., Poellot, M.R., Baumgardner, D., Rogers, D.C., Brooks, S.D., 2003. African dust aerosols as atmospheric ice nuclei. *Geophys. Res. Lett.* 30, 1732. <https://doi.org/10.1029/2003GL017410>.
- Dentener, F., Kinne, S., Bond, T., Boucher, O., Cofala, J., Generoso, S., Ginoux, P., Gong, S., Hoelzemann, J.J., Ito, A., Marelli, L., Penner, J.E., Putaud, J.-P., Textor, C., Schulz, M., van der Werf, G.R., Wilson, J., 2006. Emissions of primary aerosol and precursor gases in the years 2000 and 1750 prescribed data-sets for AeroCom. *Atmos. Chem. Phys.* 6, 4321–4344. <https://doi.org/10.5194/acp-6-4321-2006>.
- Draxler, R.R., Hess, G.D., 1998. An overview of the HYSPLIT 4 modeling system for trajectories, dispersion, and deposition. *Aust. Meteor. Mag.* 47, 295–308.
- Emori, S., Brown, S.J., 2005. Dynamic and thermodynamic changes in mean and extreme precipitation under changed climate. *Geophys. Res. Lett.* 32 <https://doi.org/10.1029/2005GL023272>.
- Engelstaedter, S., Tegen, I., Washington, R., 2006. North African dust emissions and transport. *Earth Sci. Rev.* 79 (1–2), 73–100.
- Fan, J., 2018. Substantial convection and precipitation enhancements by ultrafine aerosol particles. *Science* 359 (6374), 411–418. <https://doi.org/10.1126/science.aan8461>.
- Fan, J., Zhang, R., Li, G., Tao, W.-K., Li, X., 2007. Simulations of cumulus clouds using a spectral microphysics cloud-resolving model. *Journal of Geophysical Research: Atmospheres* 112 (D4). <https://doi.org/10.1029/2006JD007688>.
- Fan, J., Leung, L.R., DeMott, P.J., Comstock, J.M., Singh, B., Rosenfeld, D., 2014. Aerosol impacts on California winter clouds and precipitation during CalWater 2011: local pollution versus long-range transported dust. *Atmos. Chem. Phys.* 14 (1), 81–101. <https://doi.org/10.5194/acp-14-81-2014>.
- Fan, J.-W., Rosenfeld, D., Yang, Y., 2015. Substantial contribution of anthropogenic air pollution to catastrophic floods in Southwest China. *Geophys. Res. Lett.* 42 (14), 6066–6075.
- Fan, H., Zhao, C., Ma, Z., Yang, Y., 2020. Atmospheric inverse estimates of CO emissions from Zhengzhou, China. *Environmental Pollution* 267, 115164. <https://doi.org/10.1016/j.envpol.2020.115164>.
- Fan, H., Wang, Y., Zhao, C., Yang, Y., Yang, X., Sun, Y., Jiang, S., 2021a. The role of primary emission and transboundary transport in the air quality changes during and after the COVID-19 lockdown in China. *Geophys. Res. Lett.* 48(7):e2020GL091065 <https://doi.org/10.1029/2020GL091065>.
- Fan, H., Zhao, C., Yang, Y., 2021b. Impact of emissions from a single urban source on air quality estimated from mobile observation and WRF-STILT model simulations. *Air Qual. Atmos. Health* 14, 1313–1323. <https://doi.org/10.1007/s11869-021-01023-9>.
- Fast, J.D., Gustafson Jr., W.I., Easter, R.C., Zaveri, R.A., Barnard, J.C., Chapman, E.G., Grell, G.A., Peckham, S.E., 2006. Evolution of ozone, particulates, and aerosol direct radiative forcing in the vicinity of Houston using a fully coupled meteorology-chemistry-aerosol model. *Journal of Geophysical Research: Atmospheres* 111 (D21). <https://doi.org/10.1029/2005JD006721>.
- Feng, X., Mao, R., Gong, D., Zhao, C., Wu, C., Zhao, C., 2020. Increased dust aerosols in the high troposphere over the Tibetan Plateau from 1990s to 2000s. *Journal of Geophysical Research: Atmospheres* 124, e2020JD032807. <https://doi.org/10.1029/2020JD032807>.
- Fleming, Z.L., Monks, P.S., Manning, A.J., 2012. Review: untangling the influence of air-mass history in interpreting observed atmospheric composition. *Atmos. Res.* 104–105, 1–39. <https://doi.org/10.1016/j.atmosres.2011.09.009>.
- Friedl, M.A., McIver, D.K., Hodges, J.C.F., 2002. Global land cover mapping from MODIS: algorithms and early results. *Remote Sens. Environ.* 83, 287–302. [https://doi.org/10.1016/s0034-4257\(02\)00078-0](https://doi.org/10.1016/s0034-4257(02)00078-0).
- Gelaro, R., McCarty, W., Suárez, M.J., Todling, R., Molod, A., Takacs, L., Randles, C., 2017. The modern-era retrospective analysis for research and applications. Version 2 (MERRA-2). *J. Clim.* 30 (14), 5419–5454. <https://doi.org/10.1175/JCLI-D-16-0758.1>.
- Ginoux, P., Chin, M., Tegen, I., Prospero, J.M., Holben, B., Dubovik, O., Lin, S.-J., 2001. Sources and distributions of dust aerosols simulated with the GOCART model. *J. Geophys. Res. Atmos.* 106, 20255–20273. <https://doi.org/10.1029/2000JD000053>.
- Gustafson Jr., W.I., Chapman, E.G., Ghan, S.J., Easter, R.C., Fast, J.D., 2007. Impact on modeled cloud characteristics due to simplified treatment of uniform cloud condensation nuclei during NEAQS 2004. *Geophys. Res. Lett.* 34 (19) <https://doi.org/10.1029/2007GL030021>.
- Haberlie, A.M., Ashley, W.S., Pingel, T.J., 2015. The effect of urbanisation on the climatology of thunderstorm initiation. *Q. J. R. Meteorol. Soc.* 141 (688), 663–675. <https://doi.org/10.1002/qj.2499>.
- Hansen, J., Sato, M., Ruedy, R., 1997. Radiative forcing and climate response. *J. Geophys. Res.* 102 (D6), 6831. <https://doi.org/10.1029/96jd03436>.
- Heymsfield, A.J., 2007. On measurements of small ice particles in clouds. *Geophys. Res. Lett.* 34, L23812. <https://doi.org/10.1029/2007GL030951>.
- Hjelmfelt, M.R., 1982. Numerical simulation of the effects of St. Louis on mesoscale boundary-layer airflow and vertical air motion: simulations of urban vs non-urban effects. *J. Appl. Meteorol. Climatol.* 21 (9), 1239–1257. [https://doi.org/10.1175/1520-0450\(1982\)021<1239:Nstoeo>2.0.Co;2](https://doi.org/10.1175/1520-0450(1982)021<1239:Nstoeo>2.0.Co;2).
- Hong, S.-Y., Noh, Y., Dudhia, J., 2006. A new vertical diffusion package with an explicit treatment of entrainment processes. *Mon. Weather Rev.* 134 (9), 2318–2341. <https://doi.org/10.1175/mwr3199.1>.
- Hu, Y., Winker, D., Vaughan, M., Lin, B., Omar, A., Trepte, C., et al., 2009. CALIPSO/CALIOF cloud phase discrimination algorithm. *J. Atmos. Ocean. Technol.* 26 (11), 2293–2309. <https://doi.org/10.1175/2009jtecha1280.1>.
- Hu, Y., Rodier, S., Xu, K., Sun, W., Huang, J., Lin, B., Zhai, P., Josset, D., 2010. Occurrence, liquid water content, and fraction of supercooled water clouds from combined CALIOF/IR/MODIS measurements. *J. Geophys. Res.* 115, D00H34 <https://doi.org/10.1029/2009JD012384>.
- Hu, Z., Zhao, C., Huang, J., Leung, L.R., Qian, Y., Yu, H., Huang, L., Kalashnikova, O.V., 2016. Trans-Pacific transport and evolution of aerosols: evaluation of quasi-global WRF-Chem simulation with multiple observations. *Geosci. Model Dev.* 9, 1725–1746. <https://doi.org/10.5194/gmd-9-1725-2016>.
- Hu, Z., Huang, J., Zhao, C., Bi, J., Jin, Q., Qian, Y., Leung, L.R., Feng, T., Chen, S., Ma, J., 2019a. Modeling the contributions of Northern Hemisphere dust sources to dust outflow from East Asia. *Atmos. Environ.* 202, 234–243.
- Hu, Z., Huang, J., Zhao, C., Ma, Y., Jin, Q., Qian, Y., Leung, L.R., Bi, J., Ma, J., 2019b. Trans-Pacific transport and evolution of aerosols: spatiotemporal characteristics and source contributions. *Atmos. Chem. Phys.* 19, 12709–12730. <https://doi.org/10.5194/acp-19-12709-2019>.
- Hu, Z., Huang, J., Zhao, C., Jin, Q., Ma, Y., Yang, B., 2020. Modeling dust sources, transport, and radiative effects at different altitudes over the Tibetan Plateau. *Atmos. Chem. Phys.* 20, 1507–1529. <https://doi.org/10.5194/acp-20-1507-2020>.
- Hu, Z., Zhao, C., Leung, L.R., Du, Q., Ma, Y., Hagos, S., et al., 2022. Characterizing the impact of atmospheric rivers on aerosols in the western US. *Geophys. Res. Lett.* 49, e2021GL096421. <https://doi.org/10.1029/2021GL096421>.
- Hu, Z., Ma, Y., Jin, Q., Idrissa, N.F., Huang, J., Dong, W., 2023. Attribution of the March 2021 exceptional dust storm in North China. *Bull. Am. Meteorol. Soc.* E749–E755. <https://doi.org/10.1175/BAMS-D-22-0151.1>.
- Husar, R.B., Tratt, D.M., Schichtel, B.A., Falke, S.R., Li, F., Jaffe, D., 2001. Asian dust events of April 1998. *J. Geophys. Res.* 106 (D16), 18,317–18,330. <https://doi.org/10.1029/2000JD900788>.
- Iacono, M.J., Mlawer, E.J., Clough, S.A., Morcrette, J.J., 2000. Impact of an improved longwave radiation model, RRTM, on the energy budget and thermodynamic properties of the NCAR community climate model, CCM3. *Journal of Geophysical Research: Atmospheres* 105 (D11), 14873–14890. <https://doi.org/10.1029/2000JD900091>.
- IPCC, 2021. Climate change 2021: the physical science basis. In: Masson-Delmotte, V., Zhai, P., Pirani, A., Connors, S.L., Péan, C., Berger, S., Caud, N., Chen, Y., Goldfarb, L., Gomis, M.L., Huang, M., Leitzell, K., Lonnoy, E., Matthews, J.B.R., Maycock, T.K., Waterfield, T., Yelekçi, O., Yu, R., Zhou, B. (Eds.), Contribution of Working Group I to the Sixth Assessment Report of the Intergovernmental Panel on Climate Change. Cambridge University Press, Cambridge, United Kingdom and New York, NY, USA. <https://doi.org/10.1017/9781009157896> (In press).
- Jeong, M.-J., 2005. Quality and compatibility analyses of global aerosol products derived from the advanced very high resolution radiometer and Moderate Resolution Imaging Spectroradiometer. *J. Geophys. Res.* 110, D10S09. <https://doi.org/10.1029/2004JD004648>.
- Khain, A.P., Leung, L.R., Lynn, B., Ghan, S., 2009. Effects of aerosols on the dynamics and microphysics of squall lines simulated by spectral bin and bulk parameterization schemes. *J. Geophys. Res.* 114 (D22) <https://doi.org/10.1029/2009jd011902>.
- Kiesewetter, G., Borken-Kleefeld, J., Schöpp, W., et al., 2015. Modelling street level PM₁₀ concentrations across Europe: source apportionment and possible futures. *Atmos. Chem. Phys.* 15 (3), 1539–1553.
- Kok, J.F., 2011. A scaling theory for the size distribution of emitted dust aerosols suggests climate models underestimate the size of the global dust cycle. *Proc. Natl. Acad. Sci.* 108, 1016–1021. <https://doi.org/10.1073/pnas.1014798108>.
- Kranenburg, R., Segers, A.J., Hendriks, C., Schaap, M., 2013. Source apportionment using LOTOS-EUROS: module description and evaluation. *Geosci. Model Dev.* 6, 721–733. <https://doi.org/10.5194/gmd-6-721-2013>.
- Lee, S.S., Guo, J., Li, Z., 2016. Delaying precipitation by air pollution over the Pearl River Delta: 2. Model simulations. *Journal of Geophysical Research: Atmospheres* 121 (19) <https://doi.org/10.1002/2015JD024362> (11,739–711,760).
- Lee, S.S., Kim, B.G., Li, Z.-Q., 2018. Aerosol as a potential factor to control the increasing torrential rain events in urban areas over the last decades. *Atmos. Chem. Phys.* 18 (16), 12531–12550.

- Lei, M., Niyogi, D., Kishtawal, C., Pielke, R.A., Beltrán-Przekurat, A., Nobis, T.E., Vaidya, S.S., 2008. Effect of explicit urban land surface representation on the simulation of the 26 July 2005 heavy rain event over Mumbai, India. *Atmos. Chem. Phys.* 8, 5975–5995. <https://doi.org/10.5194/acp-8-5975-2008>.
- Li, Z., Zhao, X., Kahn, R., Mishchenko, M., Remer, L., Lee, K.-H., Wang, M., Laszlo, I., Nakajima, T., Maring, H., 2009. Uncertainties in satellite remote sensing of aerosols and impact on monitoring its long-term trend: a review and perspective. *Ann. Geophys.* 27, 2755–2770. <https://doi.org/10.5194/angeo-27-2755-2009>.
- Li, Z., Niu, F., Fan, J., Liu, Y., Rosenfeld, D., Ding, Y., 2011. Long-term impacts of aerosols on the vertical development of clouds and precipitation. *Nat. Geosci.* 4, 888–894. <https://doi.org/10.1038/ngeo1313>.
- Li, H., Chen, H., Wang, H., 2016. Changes in clustered extreme precipitation events in South China and associated atmospheric circulations. *Int. J. Climatol.* 36, 3226–3236. <https://doi.org/10.1002/joc.4549>.
- Li, Z., Wang, Y., Guo, J., Zhao, C., Cribb, M.C., Dong, X., 2019. East Asian study of tropospheric aerosols and their impact on regional clouds, precipitation, and climate (EAST-AIRCPC). *Journal of Geophysical Research: Atmospheres* 124, 13026–13054. <https://doi.org/10.1029/2019JD030758>.
- Lin, Y.L., 2007. *Mesoscale Dynamics*[M]. Cambridge University Press, Cambridge.
- Lin, J.-C., Matsui, T., Pielke, R.A., Kummerow, C.D., 2006. Effects of biomass-burning-derived aerosols on precipitation and clouds in the Amazon Basin: a satellite-based empirical study. *J. Geophys. Res.* 111 <https://doi.org/10.1029/2005JD006884>.
- Liu, S.-C., Fu, C.-B., Shiu, C.-J., Chen, J.-P., Wu, F.-T., 2009. Temperature dependence of global precipitation extremes. *Geophys. Res. Lett.* 36, L17702. <https://doi.org/10.1029/2009gl.040218>.
- Liu, Y.-Z., Zhu, Q.-Z., Huang, J.-P., Hua, S., Jia, R., 2019. Impact of dust-polluted convective clouds over the Tibetan Plateau on downstream precipitation. *Atmospheric Environment*, S135223101930216X-. <https://doi.org/10.1016/j.atmosenv.2019.04.001>.
- Ma, Y., Yang, Y., Wang, C., 2019. How essential of the balance between the large and small scale features to reproduce a sudden sharp turn from drought to flood using model. *Clim. Dyn.* 52 (7–8), 5013–5029.
- Ma, X., Yan, P., Zhao, T., Jia, X., Jiao, J., Ma, Q., Wu, D., Shu, Z., Sun, X., Habtemichael, B.A., 2021. Evaluations of Surface PM10 Concentration and Chemical Compositions in MERRA-2 Aerosol Reanalysis over Central and Eastern China. *Remote Sens.* 13 (7), 1317. <https://doi.org/10.3390/rs13071317>.
- Ma, Y., Hu, Z., Meng, X., Zhao, L., Dong, W., 2022a. Was the record-breaking Meiyu of 2020 enhanced by regional climate change? *Bull. Am. Meteorol. Soc.* 103 (3), S76–S82. <https://doi.org/10.1175/BAMS-D-21-0187.1>.
- Ma, Y., Hu, Z., Xie, Q., Meng, X., Zhao, L., Dong, W., 2022b. Convection-permitting modeling over the Tibetan Plateau improves the simulation of Meiyu Rainfall during the 2011 Yangtze Plain flood. *Atmos. Res.* 265 (2022), 105907.
- Ma, Y., Hu, Z., Li, C., Feng, T., Meng, X., Dong, W., 2023a. Anthropogenic climate change enhances the July 2021 super-heavy rainfall event in central China. *Bull. Am. Meteorol. Soc.* 104 (4), E736–E741. <https://doi.org/10.1175/BAMS-D-22-0141.1>.
- Ma, Y., Hu, X., Chen, Y., Hu, Z., Feng, T., Feng, G., 2023b. Different characteristics and drivers of the extraordinary Pakistan rainfall in July and August 2022. *Remote Sens.* 15, 2311. <https://doi.org/10.3390/rs15092311>.
- Miao, S., Chen, F., Li, Q., Fan, S., 2011. Impacts of urban processes and urbanization on summer precipitation: a case study of heavy rainfall in Beijing on 1 August 2006. *J. Appl. Meteorol. Climatol.* 50 (4), 806–825. <https://doi.org/10.1175/2010jamc2513.1>.
- Minnis, P., Sun-Mack, S., Young, D.F., Heck, P.W., Garber, D.P., Chen, Y., Spangenberg, D.A., Arduini, R.F., Trepte, Q.Z., Smith, B.L., Ayers, J.K., Gibson, S.C., Miller, W.F., Hong, G., Chakrapani, V., Takano, Y., Liou, K.-N., Xie, Y., Yang, P., 2011a. CERES edition-2 cloud property retrievals using TRMM VIRS and Terra and Aqua MODIS data—part I: algorithms. *IEEE Trans. Geosci. Remote Sens.* 49, 4374–4400. <https://doi.org/10.1109/TGRS.2011.2144601>.
- Minnis, P., Sun-Mack, S., Chen, Y., Khaiyer, M.M., Yi, Y., Ayers, J.K., Brown, R.R., Dong, X., Gibson, S.C., Heck, P.W., Lin, B., Nordeen, M.L., Nguyen, L., Palikonda, R., Smith, W.L., Spangenberg, D.A., Trepte, Q.Z., Xi, B., 2011b. CERES edition-2 cloud property retrievals using TRMM VIRS and Terra and Aqua MODIS data—part II: examples of average results and comparisons with other data. *IEEE Trans. Geosci. Remote Sens.* 49, 4401–4430. <https://doi.org/10.1109/TGRS.2011.2144602>.
- Mlawer, E.J., Taubman, S.J., Brown, P.D., Iacono, M.J., Clough, S.A., 1997. Radiative transfer for inhomogeneous atmospheres: RRTM, a validated correlated-k model for the longwave. *Journal of Geophysical Research: Atmospheres* 102 (D14), 16663–16682. <https://doi.org/10.1029/97JD00237>.
- Morrison, H., Thompson, G., Tatarskii, V., 2009. Impact of cloud microphysics on the development of trailing stratiform precipitation in a simulated squall line: comparison of one- and two-moment schemes. *Mon. Weather Rev.* 137 (3), 991–1007. <https://doi.org/10.1175/2008mwr2556.1>.
- Muhlbauer, A., Lohmann, U., 2009. Sensitivity studies of aerosol–cloud interactions in mixed-phase orographic precipitation. *J. Atmos. Sci.* 66 (9), 2517–2538.
- Naeger, A.R., 2018. Impact of dust aerosols on precipitation associated with atmospheric rivers using WRF-Chem simulations. *Results Phys.* 10, 217–221. <https://doi.org/10.1016/j.rinp.2018.05.027>.
- Nashwan, M.S., Shahid, S., 2022. Future precipitation changes in Egypt under the 1.5 and 2.0 °C global warming goals using CMIP6 multimodel ensemble. *Atmos. Res.* 265, 105908 <https://doi.org/10.1016/j.atmosres.2021.105908>.
- Niyogi, D., Pyle, P., Lei, M., Arya, S.P., Kishtawal, C.M., Shepherd, M., Chen, F., Wolfe, B., 2011. Urban modification of thunderstorms: an observational storm climatology and model case study for the Indianapolis urban region. *J. Appl. Meteorol. Climatol.* 50 (5), 1129–1144. <https://doi.org/10.1175/2010jamc1836.1>.
- Pistone, K., Zuidema, P., Wood, R., et al., 2021. Exploring the elevated water vapor signal associated with the free-tropospheric biomass burning plume over the southeast Atlantic Ocean. *Atmos. Chem. Phys.* 21 (12), 9643–9668. <https://doi.org/10.5194/acp-2020-1322>.
- Qian, Y., Gustafson Jr., W.L., Fast, J.D., 2010. An investigation of the sub-grid variability of trace gases and aerosols for global climate modeling. *Atmos. Chem. Phys.* 10, 6917–6946. <https://doi.org/10.5194/ACP-10-6917-2010>.
- Richardson, M.S., DeMott, P.J., Kreidenweis, S.M., Cziczo, D.J., Dunlea, E.J., Jimenez, J. L., 2007. Measurements of heterogeneous ice nuclei in the western United States in springtime and their relation to aerosol characteristics. *J. Geophys. Res.* 112, D02209. <https://doi.org/10.1029/2006JD007500>.
- Rolph, G.D., Draxler, R.R., 1993. *Real-Time Environmental Applications and Display sYstem (READY)*. Proc. Topical Meeting on Environmental Transport and Dosimetry. American Nuclear Society, Charleston, SC, pp. 113–116.
- Rosenfeld, D., 1999. TRMM observed first direct evidence of smoke from forest fires inhibiting rainfall. *Geophys. Res. Lett.* 26 (20), 3105–3108. <https://doi.org/10.1029/1999GL006066>.
- Rosenfeld, D., Lohmann, U., Raga, G.B., O’Dowd, C.D., Kulmala, M., Fuzzi, S., Reissell, A., Andreae, M.O., 2008. Flood or drought: how do aerosols affect precipitation? *Science* 321 (5894), 1309–1313. <https://doi.org/10.1126/science.1160606>.
- Shem, W., Shepherd, M., 2009. On the impact of urbanization on summertime thunderstorms in Atlanta: two numerical model case studies. *Atmos. Res.* 92, 172–189.
- Shen, L., Zhao, C., Ma, Z., Li, Z., Li, J., Wang, K., 2019. Observed decrease of summer sea-land breeze in Shanghai from 1994 to 2014 and its association with urbanization. *Atmos. Res.* 227, 198–209. <https://doi.org/10.1016/j.atmosres.2019.05.007>.
- Shen, L., Zhao, C., Yang, X., 2021. Climate-driven characteristics of sea-land breezes over the globe. *Geophys. Res. Lett.* 48, e2020GL092308 <https://doi.org/10.1029/2020GL092308>.
- Shepherd, J.M., Burian, S.J., 2003. Detection of urban-induced rainfall anomalies in a major coastal city. *Earth Interact.* 7 (4), 1–17. [https://doi.org/10.1175/1087-3562\(2003\)007<0001:Douira>2.0.Co;2](https://doi.org/10.1175/1087-3562(2003)007<0001:Douira>2.0.Co;2).
- Shepherd, J.M., Pierce, H., Negri, A.J., 2002. Rainfall modification by major urban areas: observations from spaceborne rain radar on the TRMM satellite. *J. Appl. Meteorol.* 41 (7), 689–701. [https://doi.org/10.1175/1520-0450\(2002\)041<0689:Rmbmua>2.0.Co;2](https://doi.org/10.1175/1520-0450(2002)041<0689:Rmbmua>2.0.Co;2).
- Shiu, C.-J., Liu, S.-C., Fu, C.-B., Dai, A., Sun, Y., 2012. How much do precipitation extremes change in a warming climate? *Geophys. Res. Lett.* 39, L17707. <https://doi.org/10.1029/2012gl.052762>.
- Stein, A.F., Draxler, R.R., Rolph, G.D., Stunder, B.J.B., Cohen, M.D., Ngan, F., 2015. NOAA’s HYSPLIT atmospheric transport and dispersion modeling system. *Bull. Am. Meteorol. Soc.* 96, 2059–2077. <https://doi.org/10.1175/BAMS-D-14-00110.1>.
- Su, Y., Zhao, C., Wang, Y., Ma, Z., 2020. Spatiotemporal variations of precipitation in China using surface gauge observations from 1961 to 2016. *Atmosphere* 11, 303. <https://doi.org/10.3390/atmos11030303>.
- Sun, J.-S., 2017. Differences and relationship between flash heavy rain and heavy rainfall. *Torrential Rain and Disasters* 73 (4), 609–623.
- Sun, Y., Zhao, C., 2021. Distinct impacts on precipitation by aerosol radiative effect over three different megacity regions of eastern China. *Atmos. Chem. Phys.* 21, 16555–16574. <https://doi.org/10.5194/acp-21-16555-2021>.
- Sun, E., Xu, X., Che, H., Tang, Z., Gui, K., An, L., Lu, C., Shi, G., 2019. Variation in MERRA-2 aerosol optical depth and absorption aerosol optical depth over China from 1980 to 2017. *J. Atmos. Sol. Terr. Phys.* 186, 8–19. <https://doi.org/10.1016/j.jastp.2019.01.019>.
- Sun, Y., Wang, Y., Zhao, C., Zhou, Y., Yang, Y., Yang, X., 2023. Vertical dependency of aerosol impacts on local scale convective precipitation. *Geophys. Res. Lett.* 50, e2022GL102186 <https://doi.org/10.1029/2022GL102186>.
- Tao, W.-K., Chen, J.-P., Li, Z., Wang, C., Zhang, C., 2012. Impact of aerosols on convective clouds and precipitation. *Rev. Geophys.* 50 (2) <https://doi.org/10.1029/2011rg000369>.
- Thenkabail, P., Knox, J.W., Ozdogan, M., 2012. *Assessing future risks to agricultural productivity, water resources and food security: how can remote sensing help?* Photogramm. Eng. Remote Sensing 78, 773–782.
- Thunis, P., Clappier, J., Tarrason, L., Cuvellier, C., Monteiro, A., Pisoni, E., Wesseling, J., Belis, C.A., Pirovano, G., Janssen, S., Guerreiro, C., Peduzzi, E., 2019. Source apportionment to support air quality planning: strengths and weaknesses of existing approaches. *Environ. Int.* 130, 104825 <https://doi.org/10.1016/j.envint.2019.05.019>.
- Tian, F.-Y., Zheng, Y.-G., Zhang, T., Cao, Y.-C., Sheng, J., 2017. Characteristics of environmental parameters for multi-intensity short-duration heavy rainfalls over East China. *Torrential Rain and Disasters* 36 (6), 9.
- Torres, O., 2008. OMI/Aura Near UV Aerosol Optical Depth and Single Scattering Albedo L3 1 day 1.0° × 1.0° V3. NASA Goddard Space Flight Center, Goddard Earth Sciences Data and Information Services Center (GES DISC). <https://doi.org/10.5067/Aura/OMI/DATA3003> accessed 10 July 2020.
- Trenberth, K.E., Dai, A., Rasmussen, R.M., Parsons, D.B., 2003. The changing character of precipitation. *Bull. Amer. Meteor. Soc.* 84, 1205–1217. <https://doi.org/10.1175/bams-84-9-1205>.
- Ukhov, A., Mostamandi, S., Krotkov, N., Flemming, J., da Silva, A., Li, C., et al., 2020. Study of SO2 pollution in the Middle East using MERRA-2, CAMS data assimilation products, and high-resolution WRF-Chem simulations. *J. Geophys. Res. Atmos.* 125, e2019JD031993 <https://doi.org/10.1029/2019JD031993>.
- Uno, I., Eguchi, K., Yumimoto, K., Takemura, T., Shimizu, A., Uematsu, M., 2009. Asian dust transported one full circuit around the globe. *Nat. Geosci.* 2 (8), 557–560. <https://doi.org/10.1038/ngeo583>.
- van der Werf, G.R., Randerson, J.T., Giglio, L., Collatz, G.J., Mu, M., Kasibhatla, P.S., Morton, D.C., DeFries, R.S., Jin, Y., van Leeuwen, T.T., 2010. Global fire emissions

- and the contribution of deforestation, savanna, forest, agricultural, and peat fires (1997–2009). *Atmos. Chem. Phys.* 10, 11707–11735. <https://doi.org/10.5194/acp-10-11707-2010>.
- Wang, Z., Letu, H., Shang, H., Zhao, C., Li, J., Ma, R., 2019. A supercooled water cloud detection algorithm using Himawari-8 satellite measurements. *J. Geophys. Res.-Atmos.* 124, 2724–2738. <https://doi.org/10.1029/2018JD029784>.
- Wang, X., Li, Yuqiang, Wang, M., Li, Yulin, Gong, X., Chen, Yinping, Chen, Yun, Cao, W., 2021. Changes in daily extreme temperature and precipitation events in mainland China from 1960 to 2016 under global warming. *Int. J. Climatol.* 41, 1465–1483. <https://doi.org/10.1002/joc.6865>.
- Wielicki, B.A., Barkstrom, B.R., Harrison, E.F., Lee, R.B., Smith, G.L., Cooper, J.E., 1996. Clouds and the Earth's Radiant Energy System (CERES): an earth observing system experiment. *Bull. Am. Meteorol. Soc.* 77 (5), 853–868. [https://doi.org/10.1175/1520-0477\(1996\)0772.0.CO;2](https://doi.org/10.1175/1520-0477(1996)0772.0.CO;2).
- Wienert, U., Kuttler, W., 2005. The dependence of the urban heat island intensity on latitude - a statistical approach. *Meteorol. Z.* 14, 677–686. <https://doi.org/10.1127/0941-2948/2005/0069>.
- Wu, M., Luo, Y., 2019. Extreme hourly precipitation over China: research progress from 2010 to 2019. *Torrential Rain and Disasters* 38 (5), 502–514.
- Wu, D., Wang, Z., Wang, B., Zhou, J., Wang, Y., 2011. CALIPSO validation using ground-based lidar in Hefei (31.9°N, 117.2°E), China. *Appl. Phys. B* 102, 185–195. <https://doi.org/10.1007/s00340-010-4243-z>.
- Xiao, C., Wu, P.-L., Zhang, L.-X., Song, L., 2016. Robust increase in extreme summer rainfall intensity during the past four decades observed in China. *Sci. Rep.* 6 (1) <https://doi.org/10.1038/srep38506> (38506–).
- Yang, Y., Zhao, C., Wang, Y., Zhao, X., Sun, W., Yang, J., 2021a. Multi-source data based investigation of aerosol-cloud interaction over the North China Plain and north of the Yangtze Plain. *Journal of Geophysical Research: Atmospheres* 126, e2021JD035609. <https://doi.org/10.1029/2021JD035609>.
- Yang, X., Zhao, C., Yang, Y., Fan, H., 2021b. Long-term multi-source data analysis about the characteristics of aerosol optical properties and types over Australia. *Atmos. Chem. Phys.* 21, 3803–3825. <https://doi.org/10.5194/acp-21-3803-2021>.
- Yang, X., Zhao, C., Yang, Y., Yan, X., Fan, H., 2021c. Statistical aerosol properties associated with fire events from 2002 to 2019 and a case analysis in 2019 over Australia. *Atmos. Chem. Phys.* 21, 3833–3853. <https://doi.org/10.5194/acp-21-3833-2021>.
- Yin, Y., Chen, L., 2007. The effects of heating by transported dust layers on cloud and precipitation: a numerical study. *Atmos. Chem. Phys.* 7, 3497–3505. <https://doi.org/10.5194/acp-7-3497-2007>.
- Yuan, T.-G., Huang, J.-P., Cao, J.-H., Zhang, G.-L., Ma, X.-J., 2021. Indian dust-rain storm: possible influences of dust ice nuclei on deep convective clouds. *Sci. Total Environ.* <https://doi.org/10.1016/j.scitotenv.2021.146439>.
- Zaveri, R.A., Peters, L.K., 1999. A new lumped structure photochemical mechanism for large-scale applications. *Journal of Geophysical Research: Atmospheres* 104 (D23), 30387–30415. <https://doi.org/10.1029/1999JD900876>.
- Zaveri, R.A., Easter, R.C., Fast, J.D., Peters, L.K., 2008. Model for simulating aerosol interactions and chemistry (MOSAIC). *Journal of Geophysical Research: Atmospheres* 113 (D13). <https://doi.org/10.1029/2007JD008782>.
- Zhang, Q., Streets, D.G., Carmichael, G.R., He, K.B., Huo, H., Kannari, A., Klimont, Z., Park, I.S., Reddy, S., Fu, J.S., Chen, D., Duan, L., Lei, Y., Wang, L.T., Yao, Z.L., 2009. Asian emissions in 2006 for the NASA INTEX-B mission. *Atmos. Chem. Phys.* 9, 5131–5153. <https://doi.org/10.5194/acp-9-5131-2009>.
- Zhang, Y., Luo, G., Yu, F., 2019. Seasonal variations and long-term trend of dust particle number concentration over the northeastern United States. *Journal of Geophysical Research: Atmospheres* 124, 13,140–13,155. <https://doi.org/10.1029/2019JD031388>.
- Zhao, C., Liu, X.-L., Ruby, L., Hagos, S., 2011. Radiative impact of mineral dust on monsoon precipitation variability over West Africa. *Atmos. Chem. Phys.* 11 (5), 1879–1893. <https://doi.org/10.5194/acp-11-1879-2011>.
- Zhao, Z., Pritchard, M.S., Russell, L.M., 2012. Effects on precipitation, clouds, and temperature from long-range transport of idealized aerosol plumes in WRF-Chem simulations. *J. Geophys. Res. Atmos.* 117 <https://doi.org/10.1029/2011JD016744>.
- Zhao, C., Yang, Y., Fan, H., Huang, J., Fu, Y., Zhang, X., Kang, S., Cong, Z., Letu, H., Mementi, M., 2020. Aerosol characteristics and impacts on weather and climate over the Tibetan Plateau. *Natl. Sci. Rev.* 7 (3), 492–495. <https://doi.org/10.1093/nsr/nwz184>.
- Zhao, C.-L., Ruby, L., Easter, R., Hand, J., Avise, J., 2013a. Characterization of speciated aerosol direct radiative forcing over California. *Journal of Geophysical Research: Atmospheres* 118 (5), 2372–2388. <https://doi.org/10.1029/2012JD018364>.
- Zhao, C., Chen, S., Leung, L.R., Qian, Y., Kok, J.F., Zaveri, R.A., Huang, J., 2013b. Uncertainty in modeling dust mass balance and radiative forcing from size parameterization. *Atmos. Chem. Phys.* 13 (21), 10733–10753. <https://doi.org/10.5194/acp-13-10733-2013>.
- Zhao, C., Lin, Y., Wu, F., Wang, Y., Li, Z., Rosenfeld, D., Wang, Y., 2018a. Enlarging rainfall area of tropical cyclones by atmospheric aerosols. *Geophys. Res. Lett.* 45, 8604–8611. <https://doi.org/10.1029/2018GL079427>.
- Zhao, S.-X., Sun, J.-H., Lu, R., Fu, S.-M., 2018b. Analysis of the 20 July 2016 unusual heavy rainfall in North China and Beijing. *Meteorological Monthly* 44, 351–360.
- Zhao, X., Zhao, C., Yang, Y., Sun, Y., Xia, Y., Yang, X., Fan, T., 2022. Distinct changes of cloud microphysical properties and height development by dust aerosols from a case study over Inner-Mongolia region. *Atmos. Res.* 273, 106175 <https://doi.org/10.1016/j.atmosres.2022.106175>.
- Zhong, S., Qian, Y., Zhao, C., Leung, R., Yang, X.-Q., 2015. A case study of urbanization impact on summer precipitation in the Greater Beijing Metropolitan Area: urban heat island versus aerosol effects. *J. Geophys. Res. Atmos.* 120, 10,903–10,914. <https://doi.org/10.1002/2015JD023753>.